RF-Echo: A Non-Line-of-Sight Indoor Localization System Using a Low-Power Active RF Reflector ASIC Tag

Li-Xuan Chuo, Zhihong Luo, Dennis Sylvester, David Blaauw, Hun-Seok Kim
University of Michigan
{lxchuo,zhluo,dmcs,blaauw,hunseok}@umich.edu

ABSTRACT

Long-range low-power localization is a key technology that enables a host of new applications of wireless sensor nodes. We present *RF-Echo*, a new low-power RF localization solution that achieves decimeter accuracy in long range indoor non-line-of-sight (NLOS) scenarios. RF-Echo introduces a custom-designed active RF reflector ASIC (application specific integrated circuit) fabricated in a 180nm CMOS process which echoes a frequency-shifted orthogonal frequency division multiplexing (OFDM) signal originally generated from an anchor. The proposed technique is based on time-of-flight (ToF) estimation in the frequency domain that effectively eliminates inter-carrier and inter-symbol interference in multipath-rich indoor NLOS channels. RF-Echo uses a relatively narrow bandwidth of ≤80 MHz which does not require an expensive very high sampling rate analog-to-digital converter (ADC). Unlike ultra-wideband (UWB) systems, the active reflection scheme is designed to operate at a relatively low carrier frequency that can penetrate building walls and other blocking objects for challenging NLOS scenarios. Since the bandwidth at lower frequencies (2.4 GHz and sub-1 GHz) is severely limited, we propose novel signal processing algorithms as well as machine learning techniques to significantly enhance the localization resolution given the bandwidth constraint of the proposed system. The newly fabricated tag IC consumes 62.8 mW active power. The software defined radio (SDR) based anchor prototype is rapidly deployable without the need for accurate synchronization among anchors and tags. Field trials conducted in a university building confirm up to 85 m operation with decimeter accuracy for robust 2D localization.

CCS CONCEPTS

• **Information systems → Location based services**; • **Computing methodologies → Machine learning**; • **Hardware → Wireless devices**; **Application specific integrated circuits**; **Hardware test**;

KEYWORDS

Indoor localization; Multipath; Non Line-of-sight; ASIC; RF reflection; Time-of-arrival; Neural network classification

MobiCom'17, , October 16–20, 2017, Snowbird, UT, USA.

ACM ISBN ISBN 978-1-4503-4916-1/17/10…$15.00
https://doi.org/10.1145/3117811.3117840

1 INTRODUCTION

Long-range low-power NLOS indoor localization can enable a host of location-aware Internet-of-Things (IoT) applications. Indoor navigation of public safety officials inside a building is a primary example. The localization tag built in wearable devices would significantly enhance the effectiveness of emergency evacuation, search and rescue operations. Intelligent warehouses and factories can be realized by tracking accurate locations of pallets, equipment, robots, and people in real-time to eliminate potential safety hazards while maximizing logistics efficiency. In hospitals, tracking of equipment, patients, and personnel can identify and eliminate infectious vectors, addressing a major health care issue. We envision ubiquitous localization-ready wireless tags to enable real-time tracking and logging of medical personnel / equipment interaction with patients.

A mobile tag for everyday IoT applications must be small, low power, low cost, and rapidly deployable without heavy infrastructure investment. We target a stringent power budget of <100μW in average (duty-cycled) and <100 mW peak power to fully integrate the solution in a centimeter-scale wearable tag. The localization accuracy requirement for a wide class of IoT applications is in the decimeter (10 cm) order and it must be functional in large (up to 100 m per dimension) indoor environments where NLOS scenarios are dominant with multipath-rich RF propagation. To date, there are few existing solutions that adequately address this set of challenging specifications which is critical to a wide set of localization based applications. Low-cost global positioning system (GPS) receivers [21], for example, cannot establish enough SNR to achieve better than several meters accuracy in indoor settings. WiFi or Bluetooth based indoor localization solutions are available today but their operating range is quite limited (<20 m) and their accuracy is in the order of a few meters that is insufficient to satisfy stringent public safety localization application requirements.

We introduce *RF-Echo*, a new approach in RF localization that utilizes a frequency-shifting active reflector on the tag that echoes the orthogonal frequency division multiplexing (OFDM) [26] ranging signal generated from an anchor. A frequency conversion based full duplex approach enhances the localization range and accuracy beyond the level achievable by conventional narrowband RF localization systems. We implemented the low power tag by fabricating a new custom ASIC in a 180nm CMOS technology. The anchor prototype is based on the USRP X310 [39] software defined radio (SDR) platform. Figure 1 shows the fabricated tag ASIC, the tag board, and the USRP based anchor. The tag ASIC area is 1.9×2.7mm^2 and its active power consumption at the maximum gain setting is 62.8mW. The proposed system has the following capabilities:

- **Decimeter accuracy with up to 85m localization range:** We propose a frequency domain signal processing technique

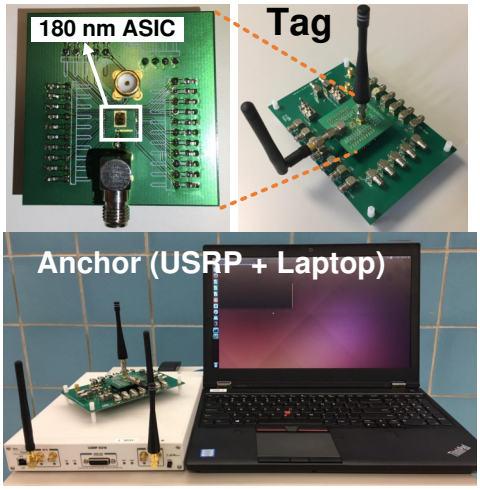

Figure 1: RF-Echo: The tag ASIC fabricated in 180nm CMOS (top), and the USRP based anchor (bottom)

that combines OFDM and neural network to accurately estimate the RF signal ToF in the frequency domain. Our measurement results show that decimeter accuracy is achievable over a ≤85 m operational distance indoor. Neural network training is based on extensive synthesized data, thus it does not require retraining after deploying the system in the field.

- **Low cost, small form factor, and low power for wearable tags:** The active reflector on the tag has a very simple architecture with minimal RF components comprising only a low noise amplifier (LNA), a bandpass filter, a frequency converter, and a power amplifier (PA). The tag does not require power-demanding high accuracy time / frequency references or sophisticated digital signal processing (DSP). The proposed technique eliminates the need for a phase-lock-loop (PLL) [30] or a crystal frequency reference for the tag IC, thus significantly lower the tag manufacturing cost.
- **Operable in NLOS and multipath-rich environments:** We investigate effective bandwidth enhancement techniques such as neural network based timing interpolation. This technique significantly enhances the effective bandwidth to analyze a multipath channel response profile in a finer resolution that is beyond the limit given in the literature [36] [7] for a narrowband system. Operating with a modest bandwidth (≤80 MHz), the proposed technique will provide sufficient resolution to distinguish line-of-sight (LOS) and NLOS paths, thus revealing the direct path distance to the target tag. This low bandwidth requirement is the key to allow RF-Echo to operate in ≤2.4GHz ISM bands. The bandwidth utilization is much lower than that of a conventional UWB system. The lower frequency signal penetrates walls better and experiences less multipath interference than conventional UWB systems.
- **Rapidly deployable, low complexity infrastructure anchors:** The bandwidth of the proposed localization signal can be easily supported by many low cost commercial off-the-shelf (COTS) RF transceivers (e.g., USRP [39]) for anchor prototyping. In addition, we eliminated the need for synchronization among anchors, while many other localization systems (e.g., [23]) require a common frequency and/or time reference among anchors. In the proposed scheme, infrastructure anchors are rapidly deployable by simply pulling them into outlets since ranging between an anchor and a tag can be performed independently without interaction among each other. Time synchronization between a tag and an anchor is also unnecessary for RF-Echo.

This paper presents the RF-Echo system architecture, algorithm, tag ASIC design, anchor implementation, and localization field trial results conducted in a university campus building. The feasibility of a narrowband decimeter-accuracy NLOS indoor localization system is demonstrated with a low-power custom ASIC implementing a low complexity analog-only architecture without a PLL or clock reference crystal. A neural network based ToF-enhancement technique is introduced to improve the reliability and accuracy of RF-Echo without an excessive bandwidth requirement. Despite the limited (1mW) transmit power available at the low-power tag, RF-Echo exhibits up to 85 m and 49 m ranging distance in realistic multipath-rich LOS and NLOS indoor scenarios respectively.

2 BACKGROUND

Before we describe RF-Echo in depth, we first briefly introduce a conventional time-of-flight (ToF) ranging method in this section. The 1-dimensional (1D) distance estimation process between the anchor and the tag is denoted by ranging. Higher dimensional localization is conducted by combining 1D ranging results from multiple anchors through multilateration process discussed in Section 3.

The ToF or time-of-arrival (ToA) based ranging techniques rely on measurements of signal travel time between an anchor and a tag with a goal to distinguish the shortest direct path arrival time from any subsequent (NLOS) multipaths [23] [15]. When sufficiently wide signal bandwidth is given, the ToF/ToA can be determined with high accuracy and since direct path always precedes the NLOS multipath, the two can be distinguished. One approach is to use an impulse-radio UWB system where very short (order of a nano second or less) pulses are transmitted and the arrival time of each pulse is estimated at the receiver to obtain the ToF of the transmitted signal [15] [41] [47] [25]. The bandwidth of an UWB pulse is inversely proportional to the pulse width and narrower pulses are preferred to obtain finer time resolution in ToF / ToA estimation. Since the RF signal travels at the speed of light, the time of flight directly maps to the distance with the relationship that 1 ns in ToF is equivalent to 30 cm in distance. The distance of the direct path in NLOS multipath-rich environments can be resolved by analyzing the first arrival signal time, not the strongest. One of key challenges to achieve decimeter level accuracy in ToF / ToA based ranging is to realize sub-nano second time resolution. In a conventional approach where the signal is sampled and then processed in the digital domain, this would require an ADC with >1G samples per second. However, such high-speed ADCs are extremely power hungry. Furthermore, as [23] shows, their cost increases exponentially with the sampling rate beyond 10MHz. Operating ADC at or above Nyquist

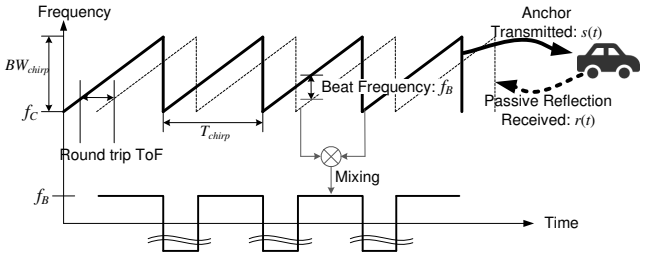

Figure 2: Operating principle of the FMCW radar. The time of flight (ToF) is proportional to the beat frequency f_B.

sampling rate (>1GHz for UWB signals) is, therefore, impractical for many low-power low-cost wireless sensor node localization applications.

While the UWB is beneficial to obtain the pulse arrival time in finer resolution, the wider bandwidth is prone to interference from different frequency bands. Relatively strong interference signals that might be present anywhere in the ultra-wide bandwidth can saturate UWB receiver amplifiers. A highly linear RF circuit for UWB is very power demanding, whereas the limited linearity of the amplifier could constraint the UWB receiver operability in the presence of in-band interferers. Moreover, due to its ultra-wide bandwidth, operating at a higher carrier frequency (typically >4GHz) is inevitable where signals experience worse pathloss and wall penetration loss, lowering its signal-to-noise ratio (SNR). According to the free-space Friis equation, 4 GHz carrier suffers 13 dB worse pathloss than a 900MHz carrier, which translates to more than 4× decrease in distance (6 dB SNR corresponds to 2× distance).

The frequency-modulated continuous-wave (FMCW) based ranging [36] [7] is a method widely used in radar systems to estimate ToF in the frequency domain. In conventional FMCW systems, the radar (i.e., anchor) transmits frequency-modulated chirp signals. The FMCW radar transmit signal, $s(t)$, is represented by equation (1) where f_c is the carrier frequency, s_f is the frequency chirp slope, and T_{chirp} is the chirp duration. The chirp bandwidth is defined as $BW_{chirp} = s_f T_{chirp}$. The operating principle of the FMCW radar is illustrated in Figure 2 .

$$s(t) = e^{j2\pi t(f_c + \frac{s_f t}{2})} \tag{1}$$

The FMCW radar estimates the distance to an object by analyzing the received signal $r(t)$ that is *passively reflected* by an object. The passively reflected signal $r(t)$ is a time-delayed (due to round-trip ToF) version of the transmitted signal. The $r(t)$ can be denoted by $h(t) * s(t) + n(t)$ where $*$ stands for convolution, $n(t)$ is the noise induced at the receiver and $h(t)$ is the round-trip channel impulse response in time domain. Note that the round-trip ToF and the ranging distance have the relationship (2), where τ_0 is the one way time-of-flight, c is the speed of light, and d is the distance to an object.

$$Roundtrip\ \ ToF = 2d/c = 2\tau_0 \tag{2}$$

For now, let us assume $h(t) = \delta(t - 2\tau_0)$ (i.e., non-multipath channel without delay spread). When the received reflection signal is mixed with the transmitted chirp signal, $r^*(t)s(t)$, a constant *beat* frequency, f_B, is observed in the down-converted (and low-pass filtered) baseband signal as in (3) (see Figure 2 for illustration). This constant beat frequency indicates the distance d to an object, as it is proportional to the round-trip ToF of the signal.

$$LPF\{r^*(t)s(t)\} = e^{j2\pi f_B t} + \tilde{n}(t),\ f_B = s_f d/c\tau_0 \tag{3}$$

3 PROPOSED SYSTEM: RF-ECHO

RF-Echo uses a full-duplex active RF reflector to estimate the range based on the round-trip ToF in frequency domain. The anchor transmits a 2.4 GHz carrier frequency ranging signal to the tag, which concurrently (in a full duplex fashion) relays the ranging signal back to the anchor with carrier frequency down-conversion to 900 MHz. Unlike a conventional RF radar, which relies on passive reflections, this active reflection with the frequency shifting approach allows full-duplex tag design without incurring complexity overhead to cancel the self-interference in the same frequency. Realizing a full-duplex system with the same transmit and receive frequency is technically challenging [4]. We have dramatically reduced the active reflector tag design complexity by intentionally shifting the reflection carrier frequency at the tag for full-duplex operation.

The main advantages of RF-Echo using a new active reflector tag are summarized as follows: 1) Increased range due to signal amplification at the tag IC. 2) Distinction between the tag reflection at 900MHz and non-targets passive reflection at 2.4 GHz. 3) Flexibility of the ranging signal scheme, allowing for application-specific waveform design. 4) Simplicity in the RF and analog tag IC design without discrete time sampling or DSP circuitry, resulting in low power, smaller chip area, low cost, and deterministic delay. 5) Lower signal pathloss and better wall penetration for the returning path from the tag because of the lowered (from 2.4GHz to 900MHz) carrier frequency.

The carrier frequency selection for the RF-Echo system is based on the trade-off study considering the tag power consumption, signal pathloss, wall penetration characteristic, and FCC regulations for different carrier frequency options. The 2.4 GHz ISM band for anchor transmission allows relatively high TX power over a wide bandwidth (80MHz). The 900 MHz band reflection is selected because of the maximum signal level specified in the FCC regulation which is the highest among sub-GHz bands for the continuous 80MHz bandwidth.

Figure 3 shows the RF-Echo system block diagram. The anchor consists of an off-the-shelf USRP SDR [39] that transmits a ≤80 MHz bandwidth ranging signal at 2.4 GHz. The tag receives this signal, shifts the carrier frequency to 900 MHz, and echoes it with a *deterministic delay*. Transmission and reception occur *concurrently at the anchor and tag*. The 2.4 GHz ISM band operation of the anchor allows up to 4W transmit equivalent isotropically radiated power (EIRP). On the other hand, the returning signal power from the tag is much lower, ≤1mW. This asymmetric power level is because of the FCC regulation (5000μV/m @ 3m at 900 MHz) and the low power constraint at the tag. RF-Echo allows a mechanism to adjust the transmit power from the anchor to limit the reflection power from the tag at 900 MHz to be under the FCC limit. Although the returning signal power is low, the sub-GHz frequency signal penetrates walls better and experiences less multipath interference than higher frequency signals.

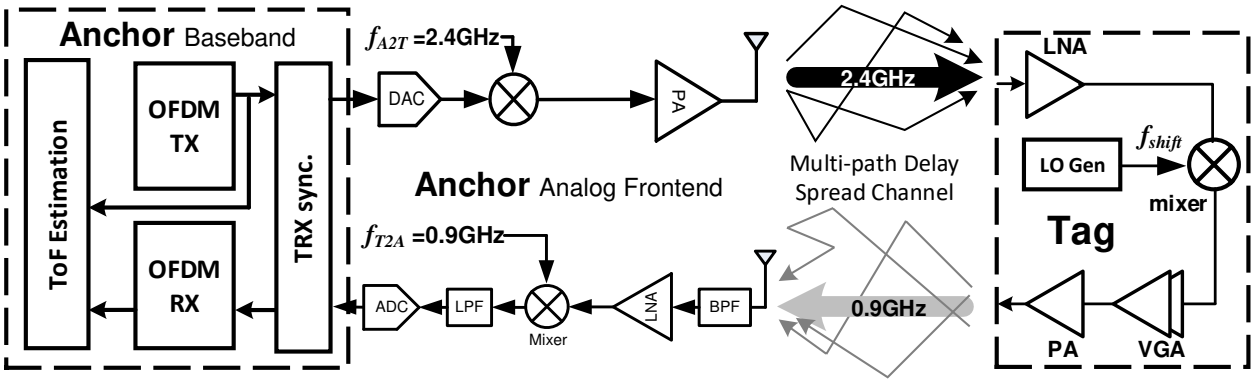

Figure 3: The overall RF-Echo system diagram. The channel impulse response is estimated in frequency domain using OFDM waveforms. The anchor broadcasts ≤80MHz OFDM signals at the 2.4GHz carrier frequency and the active reflector IC, fabricated in an 180nm CMOS process, echoes the OFDM signal with frequency down-conversion to the 900MHz carrier in a full duplex fashion.

Operating with a modest bandwidth of ≤ 80 MHz, the proposed system specification can be easily met by many low cost commercial off-the-shelf (COTS) RF transceivers and SDRs such as USRP [39] for anchor prototyping. In addition, we eliminated the need for synchronization among anchors in our scheme, while many other localization systems (e.g., [23]) require a common (i.e., cabled) frequency and/or time reference among anchors. In our scheme, infrastructure anchors are rapidly deployable since ranging between an anchor and a tag can be performed independently without interaction among each other. In fact, making anchors rapidly deployable is very crucial in some applications such as fire fighter location tracking. Time synchronization between a tag and an anchor is also unnecessary for RF-Echo.

3.1 OFDM based Ranging Waveform

The FMCW waveform discussed in Section 2 has a fundamental limit in estimating ToF when the channel has severe multipaths. Each multipath signal has a different arrival time at the anchor, thus unequal beat frequencies of random phase and magnitude multipath signals are mixed together resulting in the inter-carrier interference. Conventional FMCW systems use ultra-wide bandwidth to separate multiple beat frequencies in a high resolution [7]. To efficiently eliminate inter-carrier interference from multipaths without an excessive bandwidth requirement, we propose an OFDM based ranging signal using the datapath shown in Figure 4.

The transmitted OFDM symbol in frequency domain is defined by an $N \times 1$ complex valued vector $\mathbf{X} = [X[0], X[1], ..., X[N-1]]$ where $X[n]$ is a complex valued constellation point for the subcarrier n, and N is the number of subcarriers in the signal bandwidth (BW). The IFFT output of $\mathbf{x}$ is an $N \times 1$ complex valued vector $\mathbf{x} = [x[0], x[1], ..., x[N-1]]$, where $x[n]$ is the time domain complex sample at the time index n with Nyquist sampling rate of 1/BW (complex valued signal). To mitigate the inter-symbol interference (ISI) from the multipath delay spread, a cyclic prefix (CP) guard interval is appended to each OFDM symbol. Note that the CP guard interval must be longer than the worst case delay spread from multipaths. The CP appended signal $\mathbf{x}$ is converted to the continuous time domain signal $x(t)$ and then up-converted to 2.4 GHz for anchor transmission. This 2.4 GHz passband anchor transmit signal is denoted by $x_{A2T}(t) = x(t)e^{j2\pi f_{A2T}t}$, where f_{A2T} =2.4 GHz, as shown in Figure 3.

Accurately estimating the distance from the anchor to the tag is the central objective of RF-Echo. When the distance is d, the channel impulse response $h_{A2T}(t)$ from the anchor to the tag can be modeled as (4), where L_{A2T} is the number of multipaths, $\tau_0 = d/c$ is the one-way ToF of the RF signal to travel the distance d in the shortest path, and $h_{A2T,0}$ is the corresponding channel gain (complex valued). Other terms $h_{A2T,i}\delta(t - \tau_{A2T,i})$ are from multipath reflections satisfying $\tau_{A2T,i} > \tau_0$ with $i \geq 1$. The shortest path channel gain could be much weaker than those of other multipaths, $|h_{A2T,0}| \ll |h_{A2T,i}|,\ i > 0$, especially in NLOS conditions. Estimating τ_0 is our goal.

$$\begin{aligned} h_{A2T}(t) &= h_{A2T,0}\delta(t-\tau_0) + \sum_{i=1}^{L_{A2T}} h_{A2T,i}\delta(t-\tau_{A2T,i}), \\ h_{T2A}(t) &= h_{T2A,0}\delta(t-\tau_0) + \sum_{i=1}^{L_{T2A}} h_{T2A,i}\delta(t-\tau_{T2A,i}) \end{aligned} \tag{4}$$

Using $h_{A2T}(t)$, the received signal at the tag is denoted by $r_{tag}(t) = h_{A2T}(t) * x_{A2T}(t) + n_{tag}(t)$ where $n_{tag}(t)$ is noise added at the tag receiver front-end and the operator $*$ stands for convolution. We propose *active reflection* at the tag, where the received signal is frequency converted to 900 MHz band and sent back to the anchor in a full frequency duplex fashion. The reflected signal can be written as $x_{T2A}(t) = r_{tag}(t)e^{-2\pi f_{shift}t}$ where $f_{shift} = f_{A2T} - f_{T2A}$, and f_{T2A} =900 MHz. Here we ignore the deterministic delay of

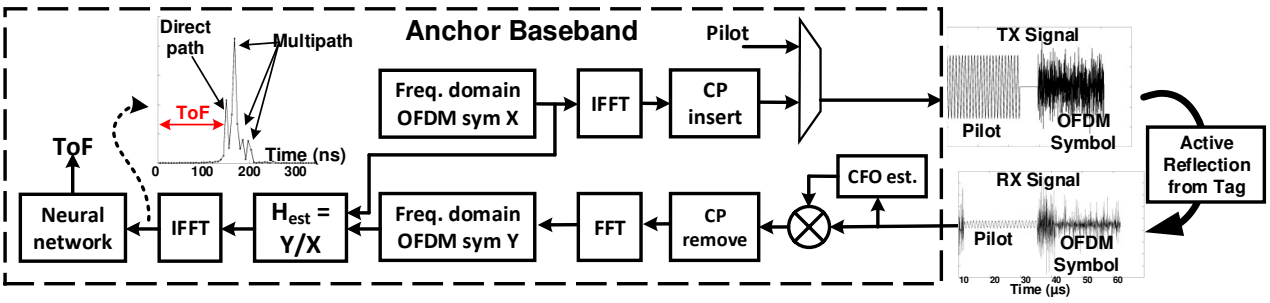

Figure 4: The OFDM based ToF estimation datapath. The OFDM ranging waveform eliminates inter-symbol and inter-carrier interferences to estimate the ToF in frequency domain. The obtained channel impulse response is fed into the neural network that extracts the ToF information from the channel impulse response.

the tag analog processing, which can be easily calibrated out at the anchor. The $x_{A2T}(t)$ reception and $x_{T2A}(t)$ transmission occur simultaneously at the tag (and at the anchor too). Unlike conventional digital systems, the active reflection tag employs *all-analog* processing as depicted in Figure 3. This approach allows the anchor to estimate the ToF τ_0 without ambiguity associated with the tag processing delay. The reflected signal $x_{T2A}(t)$ from the tag experiences channel impulse response $h_{T2A}(t)$ (4), which is different from $h_{A2T}(t)$ because of the carrier frequency difference. However, the shortest path ToF, τ_0, is common for both $h_{A2T}(t)$ and $h_{T2A}(t)$ as indicated in (4). The anchor receiver performs frequency mixing by $e^{-j2\pi f_{T2A}t}$ to bring the signal back to baseband. The baseband received signal at the anchor, therefore, can be represented by $y(t) = h_{A2T}(t) * h_{T2A}(t) * x(t) + n_{anchor}(t)$ where $n_{anchor}(t)$ is the equivalent noise at the anchor. In the frequency domain, (5) holds where $Y(f)$, $H_{A2T}(f)$, $H_{T2A}(f)$, $X(f)$ and $n_{anchor}(f)$ are Fourier transform representations of $y(t)$, $h_{A2T}(t)$, $h_{T2A}(t)$, $x(t)$, and $n_{anchor}(t)$ respectively. Before further processing, the guard interval is removed from $y(t)$ to mitigate the ISI as in conventional OFDM systems [26].

$$Y(f) = H_{A2T}(f)H_{T2A}(f)X(f) + n_{anchor}(f) \tag{5}$$

Note that the baseband signal $x(t)$ and $y(t)$ are sampled *simultaneously using the same local clock* of the anchor. By taking FFT on Nyquist sampled $y(t)$, the frequency domain received OFDM vector symbol $\mathbf{Y} = [Y[0], Y[1], \text{fi}, Y[N-1]]$ is obtained. Based on (5), channel estimation $\mathbf{H_{est}}$ in the frequency domain can be computed by (6). Unlike conventional FMCW, our method using OFDM does not suffer from inter-subcarrier interference in $\mathbf{H_{est}}$ computation. That is, $\frac{Y[j]}{X[j]}$ can be computed without interference from $i \neq j$ subcarriers because of inherent orthogonality among subcarriers in OFDM signaling [26]. The discrete time domain channel impulse response estimate $\mathbf{h_{est}} = [h[0], h[1], ..., h[N-1]]$ is obtained by taking IFFT on $\mathbf{H_{est}}$. Note that $\mathbf{h_{est}}$ is sampled at the rate of 1/BW. Our proposed system obtains the ToF τ_0 by analyzing the interpolated signal $h_{est}(t)$ of the discrete time channel impulse response such that $h_{est}(t) = h_{A2T}(t) * h_{T2A}(t) \approx interpolation(\mathbf{h_{est}})$. $h_{est}(t)$ reveals the round-trip ToF $2\tau_0$ as illustrated in Figure 4 top-left.

$$\mathbf{H_{est}} = \left[\frac{Y[0]}{X[0]}, \frac{Y[1]}{X[1]}, ..., \frac{Y[N-1]}{X[N-1]}\right] \tag{6}$$

3.2 Synchronization with Crystal-less Tags

The proposed active reflector based approach eliminates the need for time synchronization between the anchor and tag. The active reflector in the tag echoes the received signal to the anchor with a deterministic delay. All-analog design of the tag (Section 4) does not incur any sampling time ambiguity or sampling frequency offset that are inevitable in all discrete time based signal processing. Eliminating the notion of discretized time during the active reflection at the tag allows a tag design without a reference crystal to lower its manufacturing cost. Moreover, we propose a carrier frequency offset (CFO) self-calibration scheme to eliminate the conventional phase-lock loop (PLL) [30] for carrier frequency generation at the tag to further reduce its power consumption. Thus we demonstrate the feasibility of a *PLL-less and crystal-free* tag design for extremely cost-sensitive low-power tags.

The proposed CFO self-calibration is performed by sending a pilot tone, $p_{A2T}(t) = e^{j2\pi f_{pilot}t}$, before the OFDM signal $x(t)$ transmission (Figure 4, right). Any frequency mismatch f_{CFO} in the free-running LC oscillator (without a PLL) of the tag will alter the frequency of the received pilot signal (ignoring noise) to $p_{T2A}(t) = e^{j2\pi(f_{pilot}-f_{CFO})t+j\phi}$, where ϕ is the random phase mismatch. The frequency offset is estimated at the anchor by the frequency of the mixed signal; $p_{A2T}(t)p^*_{T2A}(t) = e^{j\phi}e^{j2\pi f_{CFO}t}$. The random phase offset ϕ can be ignored for ToF ranging. To validate this concept, the proposed tag IC (Section 4) is fabricated employing a free-running LC-oscillator circuit without a PLL or a reference crystal clock for frequency (f_{shift}) generation.

3.3 Neural Network based ToF Estimation

In contrast to the conventional UWB time domain ToF estimation where >1 GHz bandwidth is required to achieve cm-scale accuracy, we utilize a modest ≤80 MHz bandwidth OFDM signal and analyze the reflected signal in the frequency domain to reconstruct the time-domain channel impulse response. This ≤80 MHz constraint is from the 2.4 GHz ISM band restriction. Nyquist sampling rate

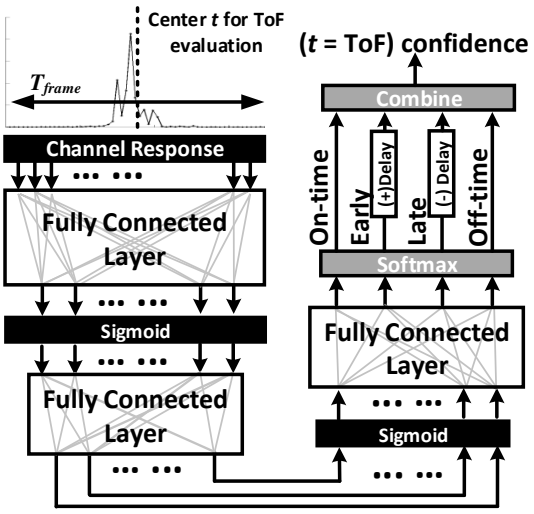

Figure 5: The proposed feedforward neural network structure. Input vector length T_{frame}=134ns (107 samples when BW = 80MHz and 10× interpolation are used). The first and second hidden layer have 48 and 16 neurons respectively. T_{offset} = 20ns for early and late neurons.

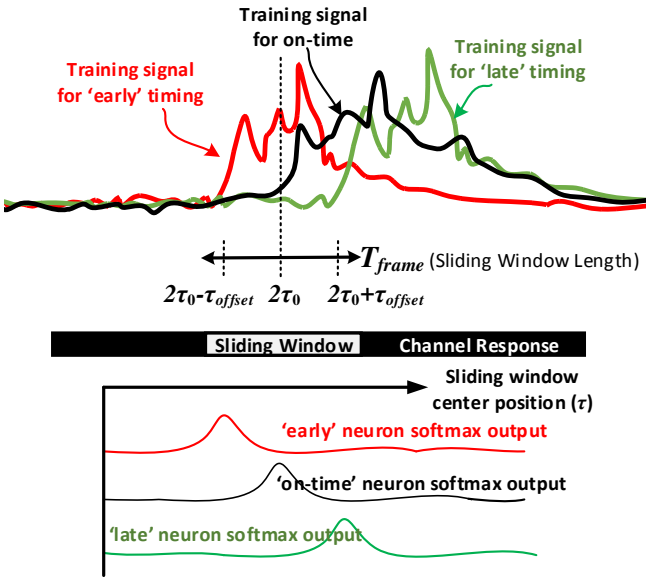

Figure 6: The proposed bootstrap aggregating method. The neural network is trained with early, on-time, and late channel impulse responses. The on-time training signal is centered at ToF $2\tau_0$. The early and late training signal are centered with a $\pm T_{offset}$ offset from ToF.

(=1/BW for a complex signal) of 80 MHz bandwidth signal indicates that the time resolution is only 12.5 ns. This is equivalent to 3.75 meter resolution for the RF signal that travels at the speed of light c, which would severely limit the accuracy of the ToF based ranging.

The accuracy limitation of this relatively low signal bandwidth of RF-Echo is overcome by a neural network based ToF estimator employed at the anchor. The proposed neural network has a fully connected feed-forward structure [17] with two hidden layers as shown in Figure 5. The neural network is trained with many (>500 k) multipath channel impulse response (CIR) training examples $h_{est}^{train}(t) = h_{A2T}^{train}(t) * h_{T2A}^{train}(t)$ that are synthesized (simulated) in Matlab. In other words, the neural network training *does not necessarily require real-world channel impulse response dataset* which is typically unavailable when RF-Echo is deployed in unknown environments. Extensive training dataset are generated using an ITU indoor channel model [20] with exponential delay profiles, randomly generated multipath taps, and random delay spreads to cover various NLOS channel scenarios. Based on the simulated dataset, feed-forward network weights are trained using a back-propagation method [17]. The neural network output is the confidence value that is (statistically) maximized when the input channel impulse response is well-aligned with the *representative shape* of the training dataset waveforms that are all centered at the ground-truth round-trip ToF. The training dataset $h_{est}^{train}(t)$ and the CIR estimation $h_{est}(t)$ signals are the interpolated (by a factor of ≥10×) version of the discrete time channel impulse response sampled at Nyquist rate. For neural network training and evaluation, we use the dB representation of the signal amplitude $20log_{10}(|h_{est}^{train}(t)|)$ and $20log_{10}(|h_{est}(t)|)$, respectively.

The training signal $h_{est}^{train}(t)$ is trimmed for the time span $t \in [2\tau_0 - \frac{T_{frame}}{2}, 2\tau_0 + \frac{T_{frame}}{2}]$, which is centered around the ground-truth round-trip ToF $2\tau_0$. T_{frame} is the training signal window size as shown in Figure 5 and 6. Note that the training signal window size is much shorter than the entire CIR time span because the neural network is only trained for the *CIR shape around the shortest ToF point*. For ToF estimation, the estimated channel impulse response $h_{est}(t)$ is fed into the trained neural network in a sliding window fashion as shown in Figure 6. When the sliding window position is τ, the $h_{est}(t)$ input window span is $t \in [2\tau - \frac{T_{frame}}{2}, 2\tau + \frac{T_{frame}}{2}]$ and the neural network evaluates if this windowed signal resembles the training dataset. The neural network output is (statistically) maximized when τ is the same as the ground-truth ToF $2\tau_0$, as illustrated in Figure 6.

To further improve the accuracy of the neural network based ToF estimation, we apply the *bootstrap aggregating* method [17] [6]. The idea is to train the neural network with several different models separately, then have all the models vote on the output to accurately estimate ToF from the $h_{est}(t)$ signal. In our proposed solution, we train the neural network not only with the training signal that is centered around the ground-truth $2\tau_0$ (i.e., *on-time* dataset) but also with other (independently generated) training dataset with a time offset τ_{offset} in ToF. The training dataset with the *early* and *late* offset has the signal span of $[2\tau_0 - \tau_{offset} - \frac{T_{frame}}{2}, 2\tau_0 - \tau_{offset} + \frac{T_{frame}}{2}]$ and $[2\tau_0 + \tau_{offset} - \frac{T_{frame}}{2}, 2\tau_0 + \tau_{offset} + \frac{T_{frame}}{2}]$ respectively as depicted in Figure 6. As the sliding window

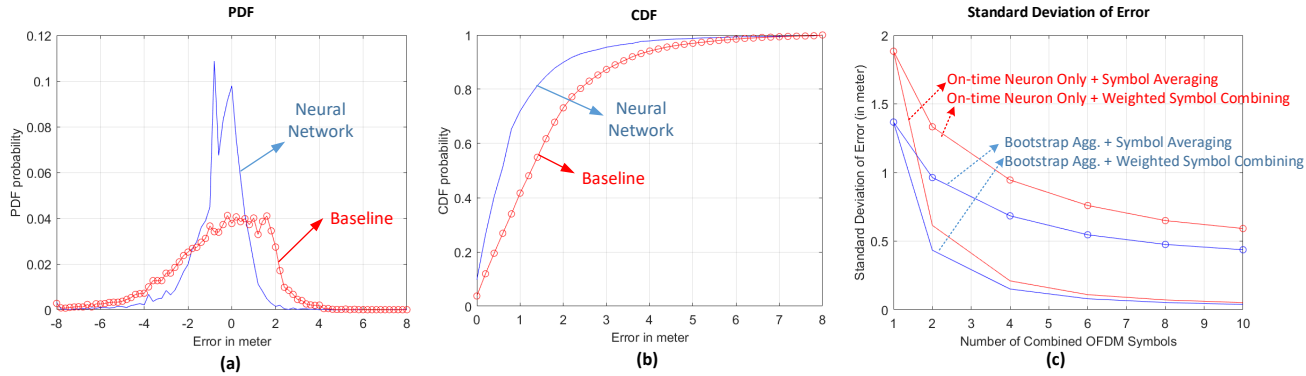

Figure 7: Ranging accuracy simulated in Matlab with 50ns delay spread multipath channels: (a) Probability density function (PDF) of errors from the proposed neural network method vs. baseline algorithm; (b) Cumulative density function (CDF) of errors, neural network vs. baseline algorithm; (c) Standard deviation of errors from multiple OFDM symbol combining: bootstrap aggregation vs. on-time neuron only, and averaging vs. confidence weighted symbol combining

position τ of the neural network input $h_{est}(t)$ changes from 0 to the maximum ToF, the neuron trained with *early* offset would generate a high confidence output first. As the slide window position τ passes by $2\tau_0$ and $2\tau_0 + \tau_{offset}$, we expect to observe a high confidence output sequentially from the *on-time* trained neuron and then from the *late* offset neuron. By combining these three confidence outputs with proper time delays, the accuracy of ToF estimate significantly improves compared to the case with *on-time* training dataset only.

Figure 7 shows the accuracy improvement from the proposed neural network algorithm compared to a hand-designed baseline algorithm. In the baseline algorithm, ToF is estimated by the timing when the power of the sample exceeds a dynamically set threshold level that is proportional to the first peak level in the channel impulse response. The threshold of the baseline algorithm is optimized over an extensive dataset for fair comparison. The Matlab simulation results in Figure 7 (a) and (b) confirm that, in a challenging 50m NLOS scenario, the neural network algorithm (error standard deviation e_{std} = 1.45m) outperforms the baseline (e_{std} = 2.09m). This result is from the single 20μs long OFDM symbol based ranging. The ranging accuracy of the neural network algorithm is further improved by the confidence-weighted symbol combining technique discussed in the next section.

3.4 Symbol Combining

The operating range target of RF-Echo is up to 100 m, which exceeds the typical operating range of popular ISM band communication standards such as WiFi. The operating range is constrained by the FCC regulation that limits the RF power transmission to be under 4W EIRP for 2.4 GHz ISM band and ≤5000μV/m @ 3 m for the 900 MHz returning path. Our tag ASIC maximum transmit power is limited to 0 dBm (1 mW). Although the 80 MHz bandwidth is significantly lower than that of UWB radios, it is still 4× wider than the legacy WiFi specification. Enhancing SNR for 80 MHz operation is critical to achieve ≈100 m range in indoor scenarios.

For RF-Echo, the complicated band-stitching technique [33] [32] can be replaced by a simple coherent signal combining of multiple OFDM symbols to enhance SNR. Although the tag and anchor are unsynchronized, a coherent channel estimation process is realized at the anchor by the *self-phase aligned processing*. That is, both transmit and receive signals are sampled using the *same local anchor clock* while the reflection delay of the tag is deterministic and constant. The frequency domain channel estimation from the i-th OFDM symbol can be represented by $\mathbf{H_{est,i}} = \mathbf{H_{est}} + \mathbf{n_i}$ where $\mathbf{H_{est}}$ is the true channel response and $\mathbf{n_i}$ is the noise vector in frequency domain. As long as the channel is stationary for multiple consecutive OFDM symbols, combining K channel estimations from consecutive OFDM symbols would increase the effective SNR by a factor of K because channel estimation from multiple measurement would add constructively (due to the self-phase aligned coherent channel estimation) while the independent noises are combined incoherently; $\sum_{i=1}^{K} \mathbf{H_{est,i}} = K\mathbf{H_{est}} + \sum_{i=1}^{K} \mathbf{n_i}$. That is, $\| K\mathbf{H_{est}} \|_2^2 = K^2 \| \mathbf{H_{est}} \|_2^2$ while $\mathrm{E}\left\{\| \sum_{i=1}^{K} \mathbf{n_i} \|_2^2\right\} = K\mathrm{E}\left\{\| \mathbf{n_i} \|_2^2\right\}$. The OFDM symbol duration is in the order of 10s of μs. Therefore, combining ≤10 OFDM symbols per localization fix does not incur unacceptable delay, while it provides up to 10dB SNR improvement.

It is also possible to combine multiple ToF estimates from the neural network output. A naive way of combining multiple ToF estimates is to use arithmetic averaging of estimated distances. The proposed neural network approach allows combining multiple ToF estimates by weighted combination using the confidence output of the final neuron. Since the activation function of the final layer of the neural network is the soft-max function, we can interpret the neural network output as the confidence weight associated with each ToF estimate. The simulation results in Figure 7 (c) show the comparison between arithmetic averaging and the weighted combining. It also shows the performance gain of the proposed bootstrap aggregation (using early, on-time and late neurons) compared to the conventional case where only on-time neuron is used. The standard deviation of 1D ranging error (e_{std}) is reduced (Matlab simulation results) from 1.45m to <0.085m by applying the confidence weighted combining of ≥6 OFDM symbols (20μs each) in

a 50ns delay spread NLOS channel. The actual measurement data using the fabricated IC is presented in Section 5.

3.5 Multilateration for 2D / 3D localization

The 2D or 3D coordinate of the tag is obtained by the multilateration process [5,8,9,38], which combines 1D ranging results from at least three anchors. It is the same process used by GPS geolocation. Given the distance estimate $\hat{d}_j$ from the j-th anchor to the tag, the tag location coordinate estimate $\mathbf{p}^*$ can be obtained by solving the optimization problem (7) [5] where $\mathbf{p}_\mathbf{j}^{\mathbf{anchor}}$ is the known coordinate of the j-th anchor, and J is the number of anchors. The optimization problem can be generalized to 2D or 3D coordinate localization cases with at least three anchors.

$$\mathbf{p}^* = \underset{\mathbf{p}}{\operatorname{argmin}} \sum_{j=1}^{J} \left(\| \mathbf{p}_\mathbf{j}^{\mathbf{anchor}} - \mathbf{p} \|_2 - \hat{d}_j \right)^2 \tag{7}$$

The optimization problem (7) is non-convex. However, it can be efficiently solved by algorithms summarized in [8,9,38]. Closed form solutions are also available [5]. The accuracy of the multilateration is directly affected by the reliability of 1D ranging performed at each individual anchor.

4 IMPLEMENTATION

4.1 Active Reflector Tag IC

The proposed active reflector tag ASIC is fabricated in a CMOS 180nm process technology. Figure 8 (a) and (b) show the schematic of the proposed tag IC. It consists of a transformer-based differential low-noise amplifier (LNA), frequency down-conversion circuits, variable gain control units (VGA), and a class-AB power amplifier (PA). Figure 8 (c) shows the fabricated chip micrograph with each component indicated. The tag IC supports a gain dynamic range of 60 dB to adjust to the received signal strength at different distances. The frequency down conversion improves the pathloss of the return path (i.e., 900 MHz reflection rather than 2.4 GHz), which lessens the transmit burden at the low power reflector, while also solving the TX/RX self-interference issue for full duplex operation. The proposed asymmetric reflective architecture simplifies tag design by shifting all signal processing complexity to the anchor and eliminating the need for time synchronization between the anchor and the tag. The transmit power is also asymmetric between the anchor and tag. Given a gain setting at the tag, the anchor can adjust its transmit power so that the returning signal power from the tag at 900 MHz is under the FCC mask.

The tag IC is designed to support a >10 dB peak-to-average-power ratio for an 80 MHz bandwidth OFDM signal with 15 – 60 dB of variable total gain. The transformer-based input matched LNA performs inherent single-ended to differential conversion, providing the doubled-balanced mixer input. This architecture is suitable for compact input matching for the 80 MHz bandwidth target [11]. To minimize the power consumption and dimension on the tag, we eliminate the usage of a crystal oscillator and the phase-locked loop (PLL) for generating the shifting frequency (f_{shift}). Instead, it uses an LC-based free-running voltage controlled oscillator (VCO) as the local oscillator (LO) and a current-commuting mixer [30] with transformer load as shown in Figure 8. PLL-less LO generation

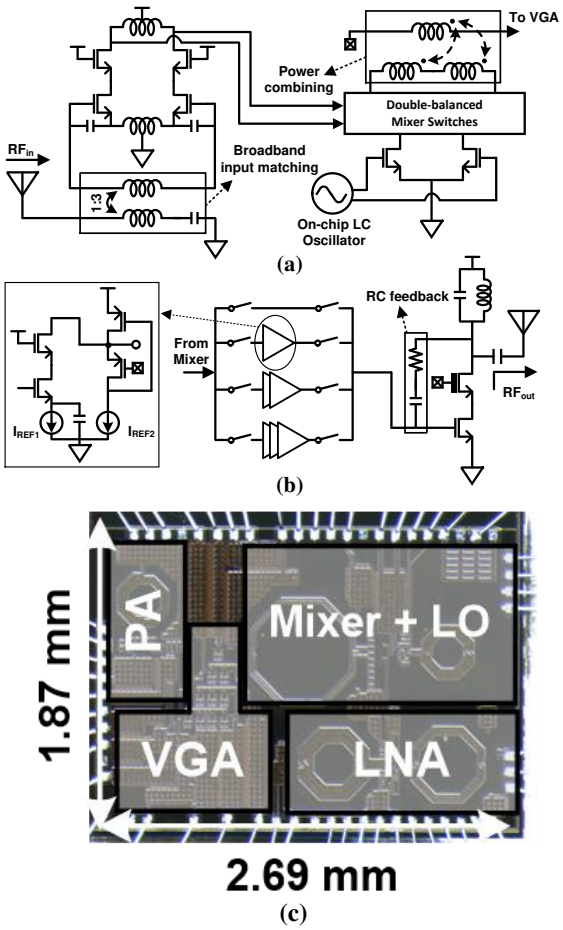

Figure 8: The active reflector ASIC: (a) LNA and mixer circuit schematic; (b) VGA and PA circuit schematic; (c) the chip die photo (fabricated in 180nm CMOS technology).

enables low power design of the tag but it is inevitable to have an inherent carrier frequency offset (CFO) that is slowly drifting over time from the target frequency. We tackle this issue using the CFO estimation/compensation technique described in Section 3. The pilot tone does not have to be inserted for every OFDM symbol as the CFO drifts slowly (at least in the order of millisecond) over time.

The transformer at the mixer output acts as a filter and a power combiner. The mixer is designed to directly drive the PA in the bypass mode with sufficient linearity. The variable gain amplifier (VGA) provides a high dynamic range and consists of 4 gain paths: high gain, mid gain, low gain, and bypass. Because of the required peak gain (60 dB) at 900 MHz and the limited on-chip area, an active inductor is used to boost the gain. The last stage is a single-ended class-AB PA with RC feedback to increase the linearity and stability.

By eliminating the off-chip crystal oscillator and PLL, the cost, complexity, and power consumption of the tag IC is significantly reduced. The measured power consumption of the tag IC is 62.8 mW when it operates with the maximum (60 dB) gain for active

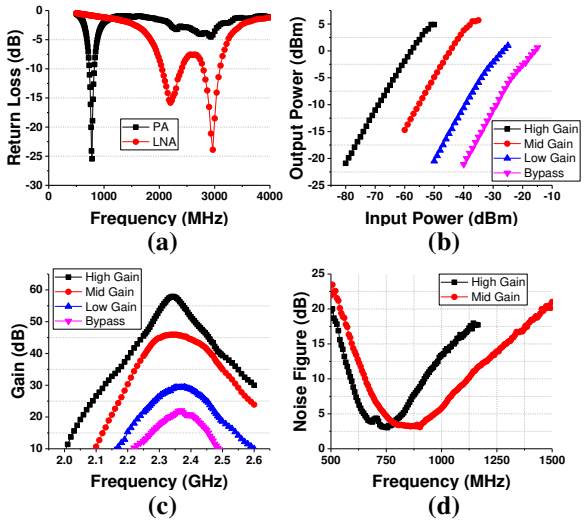

Figure 9: ASIC tag performance: (a) Input/Output impedance matching; (b) Different gain mode setting and the corresponding compression point. (c) Frequency response, showing the tag supports ≤80 MHz bandwidth at different gain modes; (d) Noise figure of the tag in high and mid gain mode.

full-duplex reflection. With a 30μs long ranging symbol (10μs pilot plus a 20μs OFDM symbol), the tag energy consumption per 1D ranging translates to 1.8μJ.

4.2 Anchor Design

For the anchor prototype (Figure 1), we use an USRP X310 [39] with an SBX-120 RF card [35] to enable the full duplex transmit and receive operation at the same time. The precise timing of the baseband OFDM transmit and receive signal sampling is controlled by a common 200 MHz main clock on the USRP FPGA. The global time stamp on the FPGA allows initiating both transmit and receive paths at the same time for the self-aligned time synchronization. The maximum OFDM signal bandwidth supported by the anchor prototype is 100 MHz. The baseband OFDM waveform generation, OFDM signal reception, pilot insertion, carrier frequency offset tracking, and neural network based post-processing are all performed on a laptop running GNU Radio [16] and Matlab software.

The 2D or 3D localization requires multiple anchors operating in a time multiplexed fashion. The accurate time synchronization among anchors, however, is not required as long as the ranging OFDM signal does not collide during the shared medium access. Each anchor can operate with a simple carrier sensing collision avoidance scheme for the medium access control. Accurate carrier frequency synchronization among anchors is also unnecessary. Any carrier frequency offset between an anchor and a tag will be resolved locally at each anchor. Without needs for accurate synchronization, anchors are rapidly deployable by simply pulling them into outlets. The 1D ranging between an anchor and a tag can be performed independently without interaction among each other. The 2D/3D localization coordinate of the target tag is established by sharing 1D ranging results among anchors and performing the multilateration process.

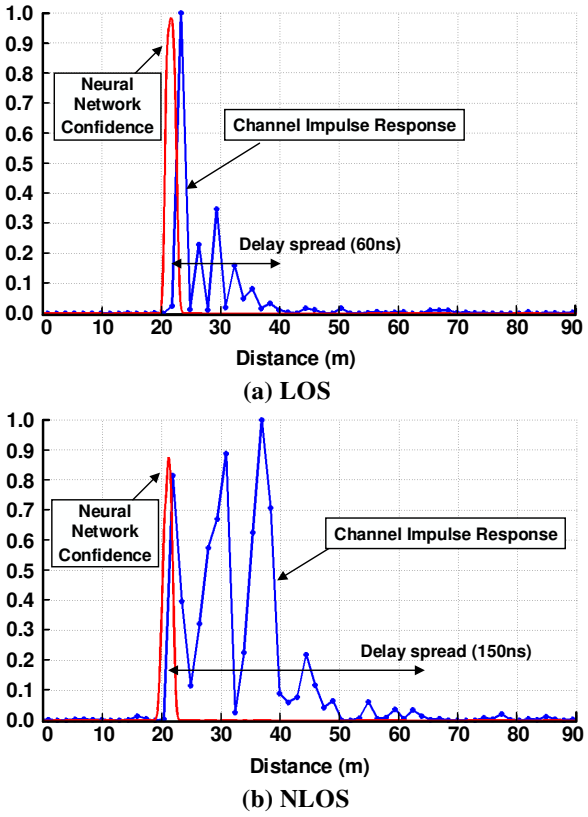

Figure 10: The anchor reconstructed channel impulse response and the neural network output confidence. For x-axis, time is converted to distance using $d/c = t$; (a) a LOS channel response; (b) a NLOS channel response.

5 EVALUATION

The measured tag sensitivity is -73 dBm when SNR is 10 dB at the anchor, which is sufficient for reconstructing the channel impulse response at 85 m LOS. The 1-dB compression point of the tag is -60 / -42 / -31 / -22 dBm for high / mid / low / bypass gain mode, respectively (Figure 9).

Figure 10 shows examples of the reconstructed impulse response $H_{est}(t)$ wirelessly captured in the field-trial with 80MHz bandwidth. Note that $H_{est}(t)$ is plotted as a function of distance (not time) by using the relationship $d/c = t$. Figure 10 (a) and (b) are channel instances in a university building for LOS and NLOS scenarios at 21.75 and 21.3 m distances respectively. Notice the severe multipath delay spread in these channel impulse responses. It also shows the neural network confidence output that accurately estimates the ToF distance 21.7 m and 21.1 m at the maximum confidence of 0.97 and 0.87 (in the scale of 0.0 – 1.0) in LOS and NLOS scenarios.

Figure 11 summarizes the RF-Echo field-trial results for ≤85.6 m LOS and ≤39.3 m NLOS indoor 1D ranging conducted in a university

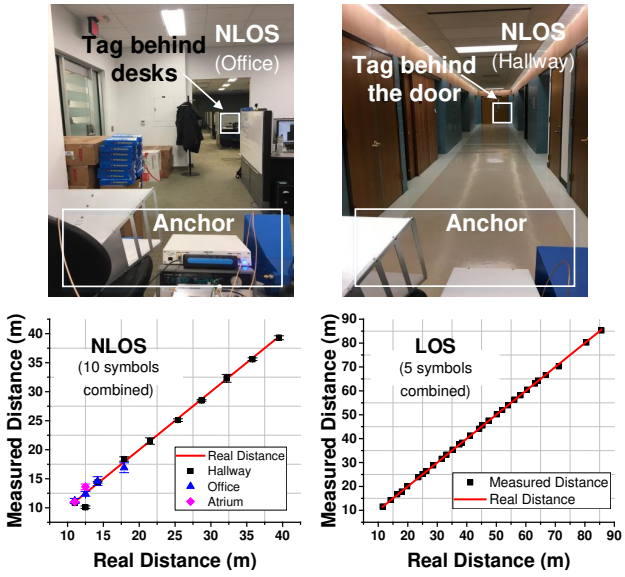

Figure 11: NLOS testing setups and the 1D LOS/NLOS ranging test results in various environments including Atrium, Office, and Hallway. The OFDM symbol length is 20μs.

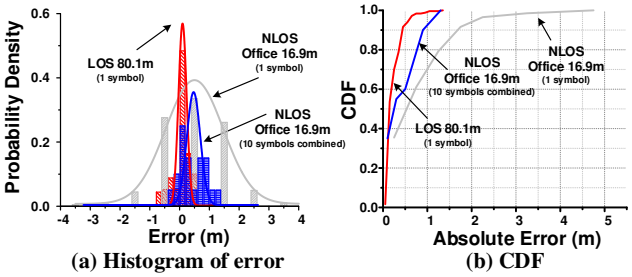

Figure 12: The 1D ranging error PDF and CDF for data points in Figure 11: (a) The error PDF with one or ten confidence-weighted OFDM symbols combining. Each symbol is 20μs long; (b) The CDF for same scenarios.

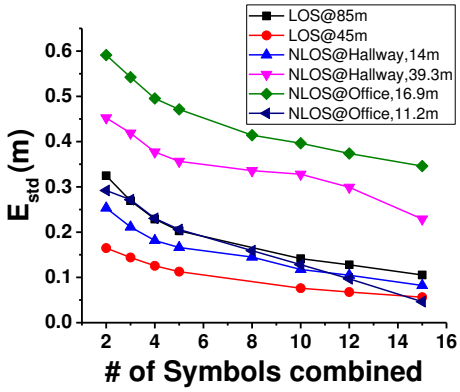

Figure 13: Error standard deviation as a function of the number of OFDM symbols combined.

campus building with testing setups shown in the same figure (top). The anchor has 30 dBm TX power and -90 dBm RX sensitivity. The operable ranging distance is limited by the tag IC reflection power $\leq$ 1mW (0dBm). The 1D ranging error histogram and the error standard deviation (e_{std}) of the same field-trials are presented in Figure 12 and 13, where the impact of neural network confidence-weighted symbol combining is shown. Each OFDM symbol is 20μs long with 1024 subcarriers.

Figure 14 shows the 2D localization map obtained from a 30×20m^2 university campus building space. The error CDF results are also shown. Anchors are black stars labeled with A_1 – A_6. The red triangles are the ground-truth tag locations, and the blue dots are estimated tag locations. Each tag location uses 10 OFDM symbols combined per estimate, and each test point has 10 estimations. Note that only A_1 – A_4 anchors are used to locate the LOS trajectory marked in the blue line. Whereas only A_4 – A_6 anchors are used to perform the NLOS localization inside a large classroom. Walls in this building are made of thick concrete and bricks. The cluster of blue dots shows the error deviation of each estimation. The error of LOS trajectory is small and almost invisible except the location around T_{14} on the map. 90^{th} percentile LOS absolute error is $\leq$ 40cm. As the tag location extends in x-dimension, the angle difference from A_1 – A_4 anchors to the tag diminishes, making the accuracy at T_{14} worse in y-dimension. This artifact is known as the dilution of precision (DOP) in a GPS system [21]. NLOS localization capability (through thick concrete walls) is demonstrated via A_4 – A_6 anchors only to locate tags (T_{15} – T_{17}) in a large classroom. Note that A_4 is outside the classroom while A_5 and A_6 are in another classroom separated by a thick concrete wall. The error of this NLOS localization is small and unrecognizable on the map.

6 RELATED WORK

One of the conventional approaches to perform RF signal based ranging is to use received signal strength indicator (RSSI) [3, 28, 34, 46]. The pathloss expression of RF signal propagation directly maps the RSSI to a distance using an inverse-square law. Due to simplicity of measuring RSSI, it has been widely adopted in WiFi or Bluetooth for ranging. Unfortunately, in NLOS or multipath-rich environments, signal fading results in large deviation in RSSI from the theoretical pathloss equation. The RSSI statistically follows a Rayleigh or log-normal distribution [29] in many practical multipath scenarios, which indicates large errors (at least a few meters) in ranging.

The angle-of-arrival (AoA) or direction-of-arrival (DoA) approach has been studied in the literature as an alternative localization method [10, 14, 27, 44]. The AoA approach performs coherent signal processing extracting the phase information of the received RF carrier signal at different antenna locations. The phase difference at different locations reveals the angle-of-arrival. Multiple AoA estimations obtained from three or more anchors provide the tag location through multilateration. Its performance, in theory, is insensitive to signal strength variation and potentially more robust than the RSSI-based method. However, employing multiple antenna arrays for AoA estimation increases the system cost, size, and complexity. Moreover, when severe multipaths exist and their signal strength is higher than or comparable to the LOS signal strength,

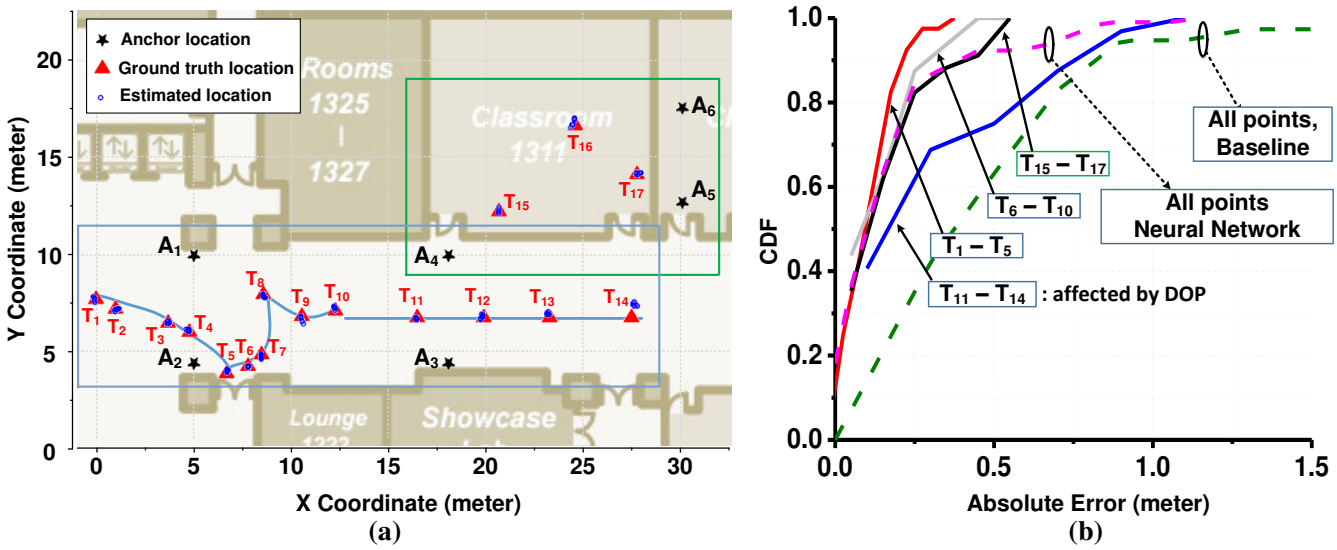

Figure 14: The 2D localization map in a 30×20m^2 university building: (a) Only $A_1 - A_4$ anchors are used to localize $T_1 - T_{15}$ along the blue trajectory. Only $A_4 - A_6$ are used to localize the NLOS positions ($T_{15} - T_{17}$); (b) The CDF of the 2D localization error. The $T_{11} - T_{14}$ has higher errors due to the diminishing differences of angles from anchors ($A_1 - A_4$) to the tag (dilution of precision, DOP). The comparison of the proposed neural network algorithm and the baseline algorithm is shown for T_1 to T_{14}.

AoA estimation could easily fail. This vulnerability to multipaths makes AoA-based methods inappropriate for many indoor localization applications. Recently, a novel synthetic aperture radar (SAR) localization system [24] is proposed to demonstrate feasibility of indoor localization in multipath environments using a commodity mobile device (a tablet PC). However, the mobile device in [24] requires accelerometer data with several seconds of motion. Its relatively low energy efficiency, high manufacturing cost per tag, and slow localization update rate limit its application for ultra-low cost, massively deployed low power tags.

With ToA / ToF based ranging capabilities, UWB radio technologies have been gaining interests since their usage in the 3.1 to 10.6 GHz band was approved by the FCC in 2002. DecaWave DW1000 [13] [12] is a commercial off-the-shelf 802.15.4a (UWB) compliant radio chipset that supports pairwise ranging between transceivers. The chipset's architecture and algorithm are not released in public. Unlike our solution, a stringent ≈10 ppm carrier frequency offset is required for system operation. The transceiver draws 393mW [13] of active power during transmit and advertises a ranging accuracy of 10 cm. Localization is performed in a packet basis with a maximum 6.8Mb/s data rate. At this data rate and a 512-byte (half of the maximum) packet length, its energy per 1D ranging is 237μJ. The tag energy in RF-Echo is only 18μJ per 1D ranging with a conservative 10 OFDM symbols combining (including the pilot, 20μs per OFDM symbol).

Other ASIC solutions [19] [31] [37] published recently are all focusing on high-power and high-accuracy LOS applications such as radar or UWB ranging. [19] uses a time-extension method to avoid the high-speed ADC needed in the UWB ranging. Although [19] achieves decent accuracy without using a GHz-ADC, this solution requires strict timing synchronization between TX and RX, severely limiting the maximum operation range. [31] utilizes careful frequency planning and sub-sampling of the incoming signal to eliminate the need for high-speed ADC. However, this paper shares a common local oscillator (LO) between the TX and RX, bypassing the issue of synchronization. [37] realizes the phase domain successive-approximation radar (SAR) with a mm-wave frequency single-carrier. This approach requires a stringent TX-RX phase-locking (homodyne detection) and results in excessive power consumption of 457 mW with 4.38 mm^2 chip area.

WASP [33] is a relatively narrow band (125MHz) ToA-based system that reports up to 30 m indoor operation with 50 cm accuracy (with a tracking algorithm from a sequential measurement). Its COTS components based design utilizes high performance RF datapath whose power consumption is at least 2 Watts. Harmonium [23] introduces a compact (1.5cm^3) low-power (75mW) tag for UWB TDoA ranging with a unique frequency-stepped receiver architecture. However, its tight timing synchronization requirement between anchors (wire-connected to each other) limits its usability for large dimension operations. All evaluation in [23] was conducted in a rather small 4.6×7.2×2.7 m^3 room space.

Chronos [40] uses channel impulse response estimation available from commodity WiFi devices for indoor localization. It stitches multiple 802.11 WiFi bands to expand the effective signal bandwidth in order to achieve higher resolution and to resolve the multipath profile using non-uniform Discrete Fourier Transform (NDFT). The proposed solution, however, assumes certain signal sparsity which might not be guaranteed in multipath-rich NLOS indoor environments. Unlike RF-Echo, Chronos requires a WiFi compliant chipset on a tag device, which would increase the tag manufacturing cost and power consumption compared to the RF-Echo tag. Its operation is based on 35 WiFi channel band stitching with 5MHz minimum

System	Technology	LOS Accuracy	NLOS Accuracy	Testing Environment Dimension	Tag Power	System Bandwidth	Signal Type	Time per Localization Fix	Energy per Localization
H. Han et al. [19]	65nm ASIC: Real time-sampling	1.9 mm	*N/A*	LOS: < 1m	70 mW @ 1m 320 mW @ 2.1m	500 MHz	Impulse	100 μs	32 μJ @ 2.1m
T. Redant et al. [31]	40nm ASIC: Equivalent time-sampling	4 mm	*N/A*	LOS: 3.6m	195 mW	2 GHz	Multi tones	20 μs	3.9 μJ @ 3.6m
Tang et al. [37]	65nm ASIC: Frequency sweep	4 mm	*N/A*	LOS: < 1m	457 mW	1.7 GHz	Sub-carrier SAR (Phase)	2 μs	0.9 μJ @ <1m
WiTrack [2]	FMCW ToF	31 cm (90%)	40 cm (90%)	LOS: 3-11m NLOS: $6 \times 5m^2$	No tag	1.69 GHz	FMCW	At least 2.5 ms	*N/A*
Harmonium [23]	UWB TDoA	31 cm (90%)	42 cm (90%)	LOS: $4.6 \times 7.2 \times 2.7m^3$ NLOS: $4.6 \times 7.2 \times 2.7m^3$	75 mW	3.5 GHz	Impulse	52 ms	3900 μJ
PolyPoint [22]	UWB ToF (DecaWave chipset)	140 cm (90%)	*N/A*	LOS: $20 \times 20m^2$	150 mW	*N/A*	Impulse	62 ms	9300 μJ
TimeDomain [1]	UWB Two-way ToF	2.1 cm	*N/A*	*N/A*	1.8 W	2.2 GHz	Impulse	6.6 ms	11880 μJ
Ubicarse [24]	SAR + Motion sensor	39 cm (median)	59 cm*** (median)	LOS: $15 \times 10m^2$ NLOS: $15 \times 10m^2$	*N/A*	*N/A*	WiFi	100 ms	*N/A*
PinIt [42]	RFID SAR	16 cm (90%)	16 cm (90%)	LOS: $6 \times 5 \times 2.2m^3$ NLOS: $6 \times 5 \times 2.2m^3$ (200 tags with 15 cm spaced)	Passive	6 MHz (UHF)	UHF RFID	5.4 s****	*N/A*
Tagoram [45]	RFID SAR	12 cm (median)	*N/A*	LOS: $1 \times 2m^2$	Passive	6 MHz (UHF)	UHF RFID	At least 33 ms	*N/A*
WASP [33]	Narrow band ToA	50 cm (85%)	50 cm (65%)	LOS: 10m NLOS: $15 \times 15m^2$	2-2.5 W	125 MHz	OFDM	100 ms	200000 - 250000 μJ
FILA [43]	802.11 RSSI + CSI*	45 cm (median)	180 cm (90%)	LOS: $5 \times 8m^2$ NLOS: $32.5 \times 10m^2$	1.6 W**	80 MHz	OFDM	16 ms	25600 μJ
Chronos [40]	802.11 WiFi + Band-stitching	14.1 cm (median)	20.7 cm (median)	LOS: $20 \times 20m^2$ NLOS: $20 \times 20m^2$	1.6 W**	20MHz × 35 overlapped ch.	OFDM	84 ms	134400 μJ
RF-Echo	**180nm ASIC: Active reflection + Neural network estimation**	**26 cm (90%)**	**46 cm (90%)**	**LOS:** $7 \times 90m^2$ **NLOS:** $30 \times 20m^2$	**62.8 mW**	**80 MHz**	**OFDM**	**20 μs per symbol**	**18 μJ (Pilot tone + 10 symbols)**

* CSI is Channel State Information on each subcarrier of 802.11 PHY layer

** Calculated based on Intel WiFi Link 5300 in RX mode [18]

*** Calculated based on reported x, y, z error

**** Including computational time

Table 1: Comparison of accuracy, dimension of field trial environment, tag power, update rate, and energy consumption per localization for a representative sampling of recently published indoor RF localization systems.

spacing, which results in a relatively slow update rate of 84 ms per measurement and the theoretical limit of ≤60 meter ranging.

Table 1 summarizes comparison between our RF-Echo system and other ASIC / COTS based systems. RF-Echo's localization accuracy, tag power, energy efficiency, tag complexity (i.e., tag cost), localization update rate, and NLOS operable range all compare favorably to other prior arts summarized in Table 1.

7 CONCLUSION

In this paper, we proposed RF-Echo, a new RF localization solution with unprecedented accuracy and energy efficiency for indoor applications. A newly fabricated active reflector ASIC is introduced to demonstrate the feasibility of low-power wireless tags that are small, low cost, and rapidly deployable without heavy infrastructure investment. The proposed approach uses OFDM signaling that effectively mitigates inter-carrier and inter-symbol interference which are common in wide bandwidth RF localization systems. Unlike conventional ToF based systems, our solution does not require strict timing and/or frequency synchronization among anchors and tags. Instead, each individual anchor uses a self-aligned timing and on-the-fly CFO tracking. This enables ultra-low cost design for the tag without a conventional PLL and clock reference crystal. The modest bandwidth of the OFDM signal allows the system to operate in 2.4 GHz and sub-1GHz bands in which the signal penetrates indoor walls better compared to the signal at a higher frequency for UWB systems. We overcome the limitation of the relative low signal bandwidth by using a neural network based ToF estimation technique. Power consumption of the active reflector tag IC is only 62.8 mW. The anchor prototype is implemented on a USRP SDR platform. Field trials conducted in a university campus building confirm that the proposed system can operate up to 85 m distance in LOS scenarios and it can provide <40 cm standard deviation of error for 1D ranging in challenging indoor NLOS scenarios. Accurate multilateration field trail results (26 cm location error in LOS and 46 cm location error in NLOS, 90% CDF) are provided to demonstrate the usability of the proposed system for various applications including indoor navigation, public safety search and rescue operations.

8 ACKNOWLEDGMENTS

The authors thank the reviewers and shepherd for their comments and feedback. This work was supported in part by TerraSwarm – an SRC program sponsored by MARCO and DARPA. This work was also supported in part by the NIST Public Safety Innovation Accelerator Program (PSIAP) Grant #70NANB17H163.

REFERENCES

[1] Time Domain PulsON 400 RCM. Online.

[2] F. Adib, Z. Kabelac, D. Katabi, and R. C. Miller. 3d tracking via body radio reflections. In *Proceedings of the 11th USENIX Conference on Networked Systems Design and Implementation*, NSDI'14, pages 317–329, Berkeley, CA, USA, 2014. USENIX Association.

[3] K. Benkic, M. Malajner, P. Planinsic, and Z. Cucej. Using rssi value for distance estimation in wireless sensor networks based on zigbee. In *2008 15th International Conference on Systems, Signals and Image Processing*, pages 303–306, June 2008.

[4] D. Bharadia, E. McMilin, and S. Katti. Full duplex radios. In *Proceedings of the ACM SIGCOMM 2013 Conference on SIGCOMM*, pages 375–386, New York, NY, USA, 2013. ACM.

[5] M. S. Brandstein, J. E. Adcock, and H. F. Silverman. A closed-form location estimator for use with room environment microphone arrays. *Speech and Audio Processing, IEEE Transactions on*, 5(1):45–50, 1997.

[6] L. Breiman. Bagging predictors. *Mach. Learn.*, 24(2):123–140, Aug. 1996.

[7] G. M. Brooker. Understanding millimetre wave fmcw radars.

[8] R. Bucher and D. Misra. A synthesizable VHDL model of the exact solution for three-dimensional hyperbolic positioning system. *Vlsi Design*, 15(2):507–520, 2002.

[9] Y. Chan and K. Ho. A simple and efficient estimator for hyperbolic location. *Signal Processing, IEEE Transactions on*, 42(8):1905–1915, 1994.

[10] H. C. Chen, T. H. Lin, H. T. Kung, C. K. Lin, and Y. Gwon. Determining rf angle of arrival using cots antenna arrays: A field evaluation. In *MILCOM 2012 - 2012 IEEE Military Communications Conference*, pages 1–6, Oct 2012.

[11] H. S. Chen, H. Y. Tsai, L. X. Chuo, Y. K. Tsai, and L. H. Lu. A 5.2-ghz full-integrated rf front-end by t/r switch, lna, and pa co-design with 3.2-db nf and +25.9-dbm output power. In *2015 IEEE Asian Solid-State Circuits Conference (A-SSCC)*, pages 1–4, Nov 2015.

[12] DecaWave. Application note: APS007. Online.

[13] DecaWave. ScenSor DW1000. Online.

[14] E. Elnahrawy, J. Austen-Francisco, and R. P. Ma. Adding angle of arrival modality to basic rss location management techniques. In *2007 2nd International Symposium on Wireless Pervasive Computing*, Feb 2007.

[15] S. Gezici, Z. Tian, G. B. Giannakis, H. Kobayashi, A. F. Molisch, H. V. Poor, and Z. Sahinoglu. Localization via ultra-wideband radios: a look at positioning aspects for future sensor networks. *IEEE Signal Processing Magazine*, 22(4):70–84, July 2005.

[16] GNU Radio Website. Online, accessed December 2014.

[17] I. Goodfellow, Y. Bengio, and A. Courville. *Deep Learning*. MIT Press, 2016.

[18] D. Halperin, B. Greenstein, A. Sheth, and D. Wetherall. Demystifying 802.11n power consumption. In *Proceedings of the 2010 International Conference on Power Aware Computing and Systems*, HotPower'10, pages 1–, Berkeley, CA, USA, 2010. USENIX Association.

[19] H. G. Han, B. G. Yu, and T. W. Kim. 19.6 a 1.9mm-precision 20gs/s real-time sampling receiver using time-extension method for indoor localization. In *2015 IEEE International Solid-State Circuits Conference - (ISSCC) Digest of Technical Papers*, pages 1–3, Feb 2015.

[20] International Telecommunication Union. Propagation data and prediction methods for the planning of indoor radiocommunication systems and radio local area networks in the frequency range 900 MHz to 100 GHz. Online.

[21] E. Kaplan and C. Hegarty. *Understanding GPS: principles and applications*. Artech house, 2005.

[22] B. Kempke, P. Pannuto, and P. Dutta. Polypoint: Guiding indoor quadrotors with ultra-wideband localization. In *Proceedings of the 2Nd International Workshop on Hot Topics in Wireless*, HotWireless '15, pages 16–20, New York, NY, USA, 2015. ACM.

[23] B. Kempke, P. Pannuto, and P. Dutta. Harmonium: Asymmetric, bandstitched uwb for fast, accurate, and robust indoor localization. In *2016 15th ACM/IEEE International Conference on Information Processing in Sensor Networks (IPSN)*, pages 1–12, April 2016.

[24] S. Kumar, S. Gil, D. Katabi, and D. Rus. Accurate indoor localization with zero start-up cost. In *Proceedings of the 20th Annual International Conference on Mobile Computing and Networking*, MobiCom '14, pages 483–494, New York, NY, USA, 2014. ACM.

[25] Z. Li, W. Dehaene, and G. Gielen. A 3-tier uwb-based indoor localization system for ultra-low-power sensor networks. *IEEE Transactions on Wireless Communications*, 8(6):2813–2818, June 2009.

[26] R. v. Nee and R. Prasad. *OFDM for Wireless Multimedia Communications*. Artech House, Inc., Norwood, MA, USA, 1st edition, 2000.

[27] R. P and M. L. Sichitiu. Angle of arrival localization for wireless sensor networks. In *2006 3rd Annual IEEE Communications Society on Sensor and Ad Hoc Communications and Networks*, volume 1, pages 374–382, Sept 2006.

[28] C. Papamanthou, F. P. Preparata, and R. Tamassia. Algorithmic aspects of wireless sensor networks. chapter Algorithms for Location Estimation Based on RSSI Sampling, pages 72–86. Springer-Verlag, Berlin, Heidelberg, 2008.

[29] T. Rappaport. *Wireless Communications: Principles and Practice*. Prentice Hall PTR, Upper Saddle River, NJ, USA, 2nd edition, 2001.

[30] B. Razavi. *RF Microelectronics*. Prentice-Hall, Inc., Upper Saddle River, NJ, USA, 1998.

[31] T. Redant, T. Ayhan, N. D. Clercq, M. Verhelst, P. Reynaert, and W. Dehaene. 20.1 a 40nm cmos receiver for 60ghz discrete-carrier indoor localization achieving mm-precision at 4m range. In *2014 IEEE International Solid-State Circuits Conference Digest of Technical Papers (ISSCC)*, pages 342–343, Feb 2014.

[32] E. Saberinia and A. H. Tewfik. Enhanced localization in wireless personal area networks. In *Global Telecommunications Conference, 2004. GLOBECOM '04. IEEE*, volume 4, pages 2429–2434 Vol.4, Nov 2004.

[33] T. Sathyan, D. Humphrey, and M. Hedley. WASP: A system and algorithms for accurate radio localization using low-cost hardware. *IEEE Transactions on Systems, Man, and Cybernetics – Part C*, 41(2), Mar. 2011.

[34] M. Saxena, P. Gupta, and B. N. Jain. Experimental analysis of rssi-based location estimation in wireless sensor networks. In *Communication Systems Software and Middleware and Workshops, 2008. COMSWARE 2008. 3rd International Conference on*, pages 503–510, Jan 2008.

[35] SBX 120 Daughterboard, Ettus Research LLC. . Online.

[36] A. G. Stove. Linear fmcw radar techniques. *IEE Proceedings F - Radar and Signal Processing*, 139(5):343–350, Oct 1992.

[37] A. Tang, G. Virbila, D. Murphy, F. Hsiao, Y. H. Wang, Q. J. Gu, Z. Xu, Y. Wu, M. Zhu, and M. C. F. Chang. A 144ghz 0.76cm-resolution sub-carrier sar phase radar for 3d imaging in 65nm cmos. In *2012 IEEE International Solid-State Circuits Conference*, pages 264–266, Feb 2012.

[38] D. Z. Thai, M. Trinkle, A. Hashemi-Sakhtsari, and T. Pattison. Speaker localisation using time difference of arrival. Technical report, DTIC Document, 2008.

[39] Universal Software Radio Peripheral (USRP), Ettus Research LLC. Online.

[40] D. Vasisht, S. Kumar, and D. Katabi. Decimeter-level localization with a single wifi access point. In *13th USENIX Symposium on Networked Systems Design and Implementation (NSDI 16)*, pages 165–178, Santa Clara, CA, 2016. USENIX Assoc.

[41] M. Verhelst, N. V. Helleputte, G. Gielen, and W. Dehaene. A reconfigurable, 0.13um cmos 110pj/pulse, fully integrated ir-uwb receiver for communication and sub-cm ranging. In *2009 IEEE International Solid-State Circuits Conference - Digest of Technical Papers*, pages 250–251,251a, Feb 2009.

[42] J. Wang and D. Katabi. Dude, where's my card?: Rfid positioning that works with multipath and non-line of sight. In *Proceedings of the ACM SIGCOMM 2013 Conference on SIGCOMM*, pages 51–62, New York, NY, USA, 2013. ACM.

[43] K. Wu, J. Xiao, Y. Yi, M. Gao, and L. M. Ni. Fila: Fine-grained indoor localization. In *2012 Proceedings IEEE INFOCOM*, pages 2210–2218, March 2012.

[44] J. Xiong and K. Jamieson. Arraytrack: A fine-grained indoor location system. In *Proceedings of the 10th USENIX Conference on Networked Systems Design and Implementation*, nsdi'13, pages 71–84, Berkeley, CA, USA, 2013. USENIX Association.

[45] L. Yang, Y. Chen, X.-Y. Li, C. Xiao, M. Li, and Y. Liu. Tagoram: Real-time tracking of mobile rfid tags to high precision using cots devices. In *Proceedings of the 20th Annual International Conference on Mobile Computing and Networking*, MobiCom '14, pages 237–248, New York, NY, USA, 2014. ACM.

[46] G. Zanca, F. Zorzi, A. Zanella, and M. Zorzi. Experimental comparison of rssi-based localization algorithms for indoor wireless sensor networks. In *Proceedings of the Workshop on Real-world Wireless Sensor Networks*, REALWSN '08, pages 1–5, New York, NY, USA, 2008. ACM.

[47] Y. Zheng, M. A. Arasu, K. W. Wong, Y. J. The, A. P. H. Suan, D. D. Tran, W. G. Yeoh, and D. L. Kwong. A 0.18um cmos 802.15.4a uwb transceiver for communication and localization. In *2008 IEEE International Solid-State Circuits Conference - Digest of Technical Papers*, pages 118–600, Feb 2008.